IET Microwaves, Antennas & Propagation

Research Article

IET Journals
The Institution of Engineering and Technology

Enhancements in mm-wave antenna measurements: automatic alignment and achievable accuracy

ISSN 1751-8725
Received on 3rd October 2016
Revised 11th January 2017
Accepted on 3rd February 2017
doi: 10.1049/iet-map.2016.0853
www.ietdl.org

Linus Boehm[1] ✉, Frank Boegelsack[1], Martin Hitzler[1], Christian Waldschmidt[1]

[1]*Institute of Microwave Engineering, Ulm University, Albert-Einstein-Allee 41, 89081 Ulm, Germany*

✉ *E-mail: linus.boehm@uni-ulm.de*

Abstract: Due to various error sources, accurate integrated antenna measurements can be difficult to achieve. This study analyses the accuracy of a measurement set-up for radiation pattern (RP), directivity and gain measurements. The main sources of uncertainty are pointed out and the overall achievable accuracy is determined. The expanded uncertainty budgets for RP, directivity and gain measurements are 0.2, 0.2 and 1.7 dB, respectively. Furthermore, the phase centre of the antenna under test (AUT) is calculated for a more accurate and faster antenna alignment. The standard deviation of the calculated phase centre position is 50 μm on each axis.

1 Introduction

As more and more hand held devices require high data rate connections and with the popularity of radar sensors, different approaches to reduce the costs and increase the data rates of the devices are being investigated. One possible approach is to use mm-wave frequencies, where the high bandwidths facilitate high data rates in communication scenarios and high-resolution radar devices. Furthermore, the short wavelengths allow to reduce the size of the required passive components significantly and make it feasible to integrate both the active and passive components of the entire sensors on a single die [1, 2]. This reduces material consumption and thus the cost of the devices. The required antennas can be realised small enough to integrate them on the same RF chip, which makes high-frequency off-chip connections unnecessary and simplifies the antenna matching.

At mm-wave frequencies, unknown material parameters and fabrication tolerances cause errors in simulation results, making them unreliable without confirming measurement data. The small wavelengths of <3 mm demand high accuracy of the measurement set-up in terms of *Rx*-*Tx* alignment and positional accuracy. Small deviations and reflections from the measurement set-up itself cause errors in the measured data. Different setups have been presented to successively increase measurement accuracy for far field [3–5] and near field antenna measurements [6–8] and to allow meaningful statements about the performance of mm-wave antennas.

To assess the accuracy of antenna measurements, the set-up presented in [9] is analysed for radiation pattern (RP), directivity and gain measurements as shown in [10, 11]. Different error sources were identified and are presented in Section 2 and an uncertainty analysis as described in Section 3 was performed for different antenna measurements.

Additionally, the phase centre of the AUT is determined in Section 4 based on a far field measurement to correct misalignment errors between AUT and Rx antenna and thus improving the accuracy for different measurement scenarios. Furthermore, this allows an automated alignment process between AUT and *Rx* antenna, which facilitates the measurement process and increases measurement repeatability.

The set-up comprises a robotic arm, which moves the *Rx* antenna around the AUT and triggers measurements at the desired locations. The type of measurement (far field, near field, polarisation and extrapolation) as well as the different parameters (frequency, resolution and measurement surface) can be specified through a graphical python user interface.

The setup is shown in Fig. 1 and a block diagram in Fig. 2. Converter modules are used to extend the frequency range of the network analyser up to 300 GHz. The measurements that are shown in this paper are spherical far field measurements (Fig. 3) at 280 GHz.

2 Error sources

To evaluate the overall accuracy of the set-up all possible error sources that can influence the measurement results have to be identified. The error sources that were taken into account for this study are listed in Table 1. The third column indicates if RP, directivity (D) or gain (G) measurements are affected by a particular error source. A detailed description of the different error sources can be found in [10].

A horn antenna at 280 GHz was used for the RP and directivity analysis and an integrated antenna for the gain measurement. The gain was calculated with the gain comparison method using a horn antenna as a reference.

3 Uncertainty budget

The uncertainty analysis for the different measurement types was performed as described in [12]. Different error sources x_i were identified and their individual impact on the measured quantity y was determined by calculating the sensitivity c_k of y towards a particular error source x_k:

$$c_k = \frac{\delta y}{\delta x_k}. \tag{1}$$

This can be done with either propagation of error or through repeated measurements.

When the relation between an error source and the measured quantity is known, propagation of error can be applied. By calculating the impact of the maximum expected deviation of x_k on the result y, the sensitivity c_k can be determined. This approach was used for the sensitivity of gain measurements towards a faulty measurement distance, as the resulting error can be calculated using the free space attenuation as shown in [10].

For most error sources x_i the relation between the source and the measurement result y is not known. To determine the sensitivity the result of a reference measurement y_{ref} was compared with a second measurement, where one error source x_k was deliberately

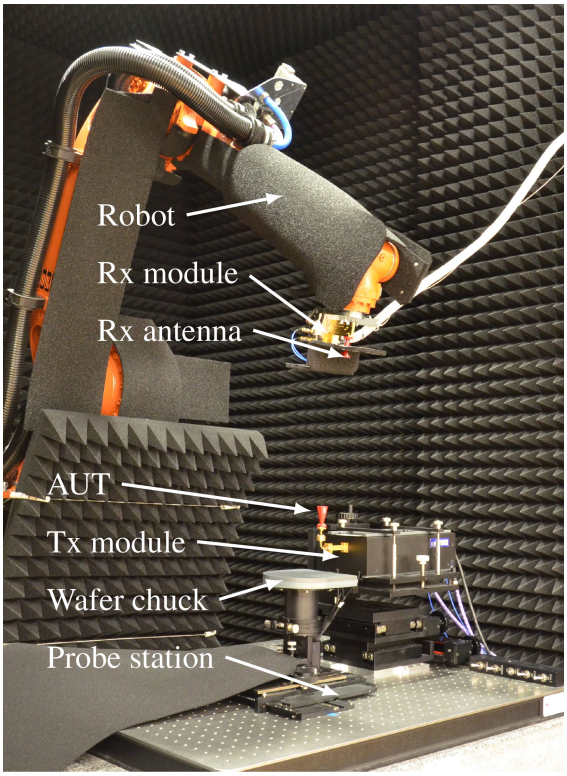

Fig. 1 *Measurement setup with robot, converter module and probe station*

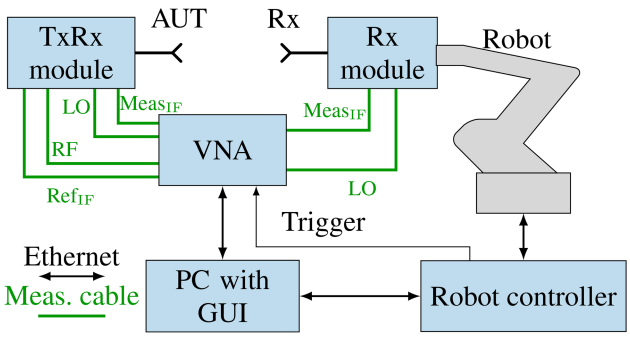

Fig. 2 *Schematic of the measurement set-up*

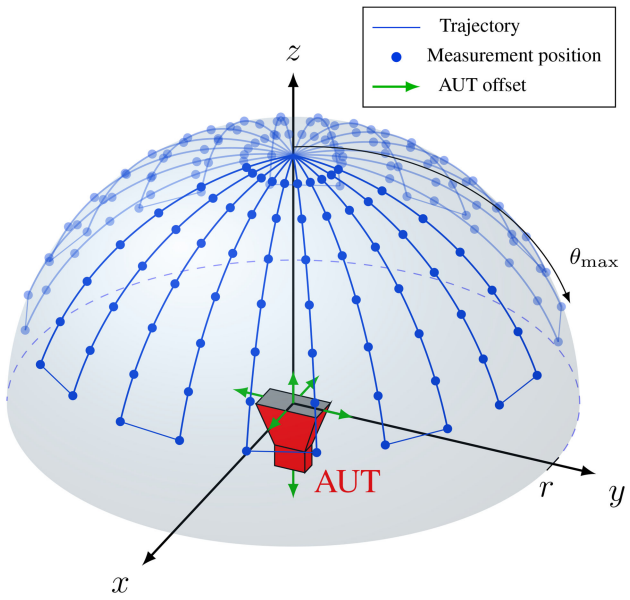

Fig. 3 *Far-field measurement trajectory with a horn antenna as AUT*

changed by the uncertainty of this error source $u(x_k)$, while the other error sources $x_{j,j\neq k}$ stayed constant. This yields a faulty measurement result y_{err} with an error caused by the change of x_i. Assuming a linear relation between $u(x_i)$ and the measurement result as a first-order approximation due to the small shifts of the nominal value, the sensitivity can be calculated with

$$c_k = \frac{|y_{\mathrm{err}}(x_i) - y_{\mathrm{ref}}(x_i)|}{u(x_i)}. \tag{2}$$

As it would be an overestimation of the measurement uncertainty if the maximum uncertainty for all x_i was assumed, the overall uncertainty budget $u_c(y)$ is calculated with the standard deviations of the error sources s_{x_i}

$$u_c(y) = \sqrt{\sum_{i=1}^{N} (c_i \cdot s_{x_i})^2}, \tag{3}$$

where N is the total number of error sources. The standard deviation of an error source x_i depends on the distribution of x_i. For this analysis, a normal distribution for all errors was assumed. For normal distributed errors, the standard deviation of an error source can be determined with

$$s_{x_i} = \frac{1}{3} u(x_i). \tag{4}$$

For a higher level of confidence, the expanded uncertainty budget $U_c(y)$ is defined

$$U_c(y) = k \cdot u_c(y). \tag{5}$$

For this analysis, $k = 2$ was used, which corresponds to a confidence of 95%. This means that there is a 95% probability that the difference between the measured value and the true value is smaller than $U_c(y)$.

4 Automatic alignment

A laser range finder, which is mounted to the robot, is used to manually align the AUT and the *Rx* antenna. This requires the user to stepwise move the robot and visually check the laser position until it points on the AUT, which is not only time consuming, but the accuracy is also limited due to the diameter of the laser and its distance measurement accuracy. As a consequence, the AUT location cannot be determined exactly, which is especially problematic for high gain antennas, where the amplitude of the received signal changes quickly over the measurement position, for integrated antennas, which can be much smaller than the laser diameter itself, and for near field measurements, where accurate phase information is required for an accurate far-field calculation. Using the laser range finder, the AUT location has a standard deviation of $s_{x_{x-\mathrm{pos}}} = 0.5$ mm, $s_{x_{y-\mathrm{pos}}} = 0.5$ mm and $s_{x_{z-\mathrm{pos}}} = 0.67$ mm [10] (AUT offsets indicated in Fig. 3).

To determine the AUT position with higher accuracy and to simplify the alignment procedure for the user, the phase centre of the AUT can be calculated based on an initial far-field measurement. The calculated phase centre can then be used as an origin for the antenna measurement.

Most antenna measurement setups measure the RP of a turning AUT with a static probe antenna, which is why the offset between the rotation centre of the measurement and the phase centre of the AUT is of particular interest. In [13, 14], this critical offsets was determined and corrected, but this offset is not present in setups, where the probe antenna is rotated around a static AUT. The flip-test method of [15–17] uses two electrical field measurements to determine the offset of the phase centre with respect to the reference antenna and the rotational axes of the measurement setup. This method, however, has not been applied to 3D-

Table 1 Uncertainty budgets

#	Source of uncertainty x_i	Affected measurements	Uncertainty (±)	Radiation pattern		Directivity		Gain	
			$u(x_i)$	c_i	s_{x_i}	c_i	s_{x_i}	c_i	s_{x_i}
1	AUT pos x	RP/D/G	150 µm	0.024 dB/mm	50 µm	0.004 dB/mm	50 µm	0.006 dB/mm	50 µm
2	AUT pos y	RP/D/G	150 µm	0.248 dB/mm	50 µm	0.008 dB/mm	50 µm	0.041 dB/mm	50 µm
3	AUT pos z	RP/D/G	150 µm	0.041 dB/mm	50 µm	0.003 dB/mm	50 µm	0.028 dB/mm	50 µm
4	AUT tilt	RP/D/G	0.125°	1.369 dB/°	0.04 °	0.06 dB/°	0.04 °	0.165 dB/°	≈0
5	AUT mismatch	G		—	—	—	—	≈0	—
6	Rx tilt	—	0.1°	—	—	—	—	—	—
7	Rx length	—	100 µm	—	—	—	—	—	—
8	Rx phase centre	—	5 mm	—	—	—	—	—	—
9	Rx gain	—	0.2 dB	—	—	—	—	—	—
10	REF gain	G	0.1 dB	—	—	—	—	1	0.033 dB
11	REF tilt	G	0.125°	—	—	—	—	1.369 dB/°	0.04°
12	REF phase centre	G	5 mm	—	—	—	—	0.012 dB/mm	1.67 mm
13	REF mismatch	G		—	—	—	—	≈0	—
14	connectors	G	0.4 dB	—	—	—	—	1 dB/dB	0.133 dB
15	trigger position	RP	350 µm	1 dB/dB	0.038 dB	1 dB/dB	0.012 dB	—	—
16	cable flex	RP						—	—
17	noise	RP/G						1 dB/dB	0.084 dB
18	AUT-Rx-polarization	RP/D/G	0.1°	—	≈0	—	≈0	—	≈0
19	distance	G	350 µm	—	—	—	—	≈0	≈0
20	multiple reflections	RP/D/G		1 dB/dB	0.049 dB	1 dB/dB	0.036 dB	1 dB/dB	0.833 dB
21	ϕ resolution (3°)	D		—	—	1 dB/dB	0.005 dB	—	—
22	θ resolution (0.25°)	RP/D		≈0	—			—	—
23	max θ	D		—	—	1 dB/dB	0.009 dB	—	—
24	amplitude drift (1 h)	D/G	0.025 dB	—	—	—	≈0	—	≈0
25	vector network analyzer crosstalk	RP/D	112 nV_{rms}	—	≈0	—	≈0	—	≈0
26	receiver non-linearity	RP/D/G		1 dB/dB	0.049 dB	1 dB/dB	0.09 dB	—	≈0
27	absorber placement	RP/D/G		—	≈0	—	≈0	—	≈0
expanded uncertainty $U_c(y)$ (95% confidence):				0.2 dB		0.2 dB		1.7 dB	

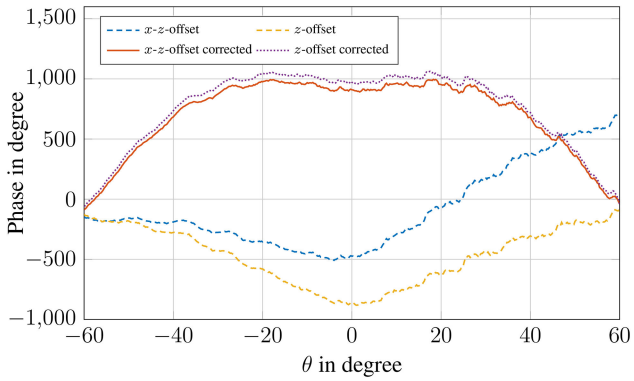

Fig. 4 *Correction of the measured phase in the x-plane based on the calculated phase centre*

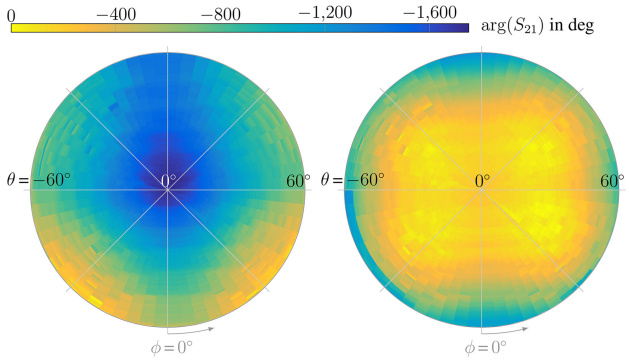

Fig. 5 *Phase of a 3D horn antenna measurement at 280 GHz. x-offset = 1.5 mm, z-offset = 5 mm*

measurements and requires two measurements to determine the offset in one plane. In this paper, a different approach is proposed.

For an isotropic radiator the measured phase would be constant over a spherical measurement surface, if the phase centre of the antenna is in the origin of the measurement. Alignment offsets of the antenna in x- and y-direction cause asymmetries of the measured phase in the respective plane as shown in Figs. 4 and 5*a*. An offset in z-direction introduces a symmetrical slope (± cosine shape, depending on the direction of the offset, Fig. 4).

The phase centre of a real antenna depends on the viewing angle and the frequency and is therefore not constant on a spherical scanning surface. However, asymmetries in the measured phase pattern can be used to determine the phase centre of a real antenna. For the calculation, the origin $\boldsymbol{o}$ of a measurement at the distance r was moved by recalculating the phase at each measurement position $\boldsymbol{p}_i = (x_{p_i}, y_{p_i}, z_{p_i})$ depending on the path length to the moved origin $\boldsymbol{o}'$.

First, the distance between $\boldsymbol{p}_i$ and the moved origin $\boldsymbol{o}'$ was calculated as

$$r' = \left|\boldsymbol{p}_i - \boldsymbol{o}'\right|. \tag{6}$$

The path difference for each measurement point between measurement distance r and the distance with the updated origin r' is

$$\Delta r = r - r'. \tag{7}$$

With the wave number $k = 2\pi/\lambda$, this corresponds to a phase change of

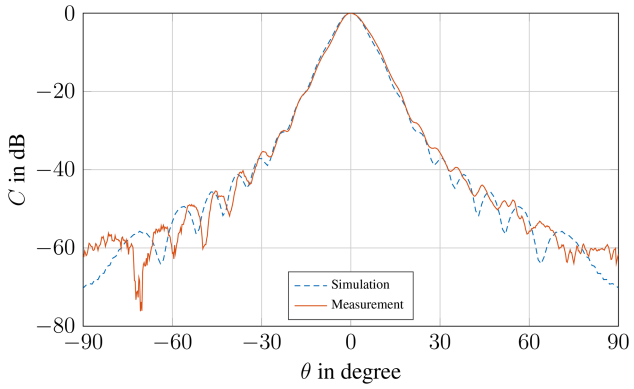

Fig. 6 *Measurement of a horn antenna in the H-plane at 280 GHz*

$$\Delta\phi = k\Delta r\,. \tag{8}$$

Therefore, the updated phase of the measured signal is

$$S'_{21} = S_{21}\cdot \mathrm{e}^{-\mathrm{j}\Delta\phi}\,. \tag{9}$$

The phase centre is determined by minimising the standard deviation of $\arg(S'_{21})$ with respect to $\boldsymbol{o}'$ for two orthogonal cuts. A measurement in the x–z planes yields an offset for the x- and z-direction (Δx, Δz_x) and likewise a y and z planes measurement for the y- and z-direction (Δy, Δz_y). The location of the phase centre $\boldsymbol{c}$ was calculated as

$$\boldsymbol{c} = \boldsymbol{o} + \left(\Delta x, \Delta y, \frac{\Delta z_x + \Delta z_y}{2}\right). \tag{10}$$

The z-location of the phase centre was averaged from the E- and H-planes result, as the phase centre location changes depending on the regarded plane [18].

The phase centres were calculated for both measurements shown in Fig. 4. The criterion for the evaluation region was that the RP was within 40 dB of the main lobe in the H-plane. The measured phase was then corrected based on the calculated phase centre position. The calculated phase centres for both measurements were within 150 µm and the corrected phase of the measurement results $\arg(S'_{21})$ shows high agreement. The offset in x-direction was 1.5 mm for the first measurement and 5 mm in z-direction for both measurements. While the mean phase difference between the two measurements was almost 400°, the mean difference was reduced to ∼50° by the correction. Fig. 5 shows the 3D phase of the same x–z offset measurement as well as the polar plot of the corrected phase. Before the phase correction the maximum phase difference was around 1600° and around 800° after the correction.

To evaluate the uncertainty of the phase centre determination, the standard deviation of the calculated phase centre was calculated for multiple horn antenna measurements with different offsets in x-, y- and z-direction and different angular evaluation regions. The measurement distance was 250 mm. The offset position was changed between 1 and 5 mm and the magnitude criterion for the evaluation range was varied between 10 and 50 dB within the main lobe in the H-plane. The standard deviation was <150 µm in the x and y planes, which is significantly better than the achieved accuracy with the laser range finder. While the phase centre in x- and y-directions was constant over the evaluation range, the z-location changed and had a comparatively large standard deviation of 4.6 mm. For larger θ ranges, the phase centre moves further into the antenna, which is why it is important to use the same evaluation range for repeatable measurements. For an evaluation region within 40 dB of the main lobe, the standard deviations were <50 µm for all three axes.

To validate the procedure, a post processed phase pattern was compared with a measurement result around the same origin. A 1.5 mm x-offset measurement was used for post-processing. The mean phase error between the post-processed results and the measurement was <30° in the critical x and z planes. Therefore, a similar agreement as between the two post-processed results shown in Fig. 4, where the standard deviation was 50°, was achieved.

The phase centre calculation works especially well for setups without any strong reflectors. When measuring integrated antennas that are fed with wafer probes, the phase centre of the superimposed field can differ from the phase centre of the AUT.

5 Measurement uncertainty budgets

A standard gain horn antenna was used as AUT for the directivity, RP analysis and as a reference antenna for gain measurements, while an integrated antenna was used as AUT.

5.1 Radiation pattern

As the measurement set-up is intended for integrated antennas, 30 dB within the main lobe of the horn antenna were taken into account for the RP uncertainty to cover the dynamic range of typically low gain integrated antennas. Fig. 6 shows the comparison of simulation and measurement results for the AUT.

To isolate the influence of the error source under evaluation from random errors 10 measurement were averaged for each error source. The impact of random errors was determined by calculating the standard deviation between the 10 reference measurements. An example on how the sensitivity towards a specific error source was calculated can be found in [10] for an AUT offset in y-direction.

For this setup and this AUT, the resulting extended uncertainty budget is 0.2 dB (95% confidence). Therefore, the automatic alignment based on the calculated phase centre improved the accuracy by around 0.1 dB compared to [10]. However, the accuracy can change depending on the setup and AUT.

5.2 Directivity

By integrating over the measured RP $C(\theta, \phi)$, the directivity can be calculated as

$$D = \frac{4\pi}{\int_{\phi=0}^{2\pi}\int_{\theta=0}^{\pi} C^2(\theta,\phi)\sin\theta\,\mathrm{d}\theta\,\mathrm{d}\phi}\,. \tag{11}$$

As the integration averages over all measurement points, both AUT offsets and noise have a smaller impact on the measurement accuracy compared to RP measurements, leading to lower sensitivities towards error sources #1–#5 and #16–#18.

A more detailed discussion of other error sources can be found in [10]. Due to the low sensitivity towards misalignment, the accuracy improvements through the phase centre calculation are negligible for directivity measurements. The extended uncertainty budget is 0.2 dB.

5.3 Gain

The AUT for the gain measurement was an integrated antenna shown in Fig. 7. The gain was determined with the gain comparison method and a standard gain horn antenna was used as a reference antenna. The gain of the AUT is determined by comparing the measured S_{21} to the reference antenna. The effect of connectors that differ between the two measurements has to be removed:

$$G_{\mathrm{AUT}}|_{\mathrm{dBi}} = S_{21,\mathrm{AUT}}|_{\mathrm{dB}} - S_{21,\mathrm{ref}}|_{\mathrm{dB}} + G_{\mathrm{ref}}|_{\mathrm{dBi}} - S_{21,\mathrm{con}}|_{\mathrm{dB}}\,. \tag{12}$$

For prototyping purposes integrated antennas are often fabricated without any active circuitry. These standalone antennas have to be fed with wafer probes [19], which have to be taken into account for $S_{21,\mathrm{con}}$. Additionally, the losses on the chip and the influence of a waveguide bend that was used for the reference antenna have to be considered:

$$S_{21,\mathrm{con}}|_{\mathrm{dB}} = S_{21,\mathrm{probe}}|_{\mathrm{dB}} + S_{21,\mathrm{chip}}|_{\mathrm{dB}} - S_{21,\mathrm{WGB}}|_{\mathrm{dB}}\,. \tag{13}$$

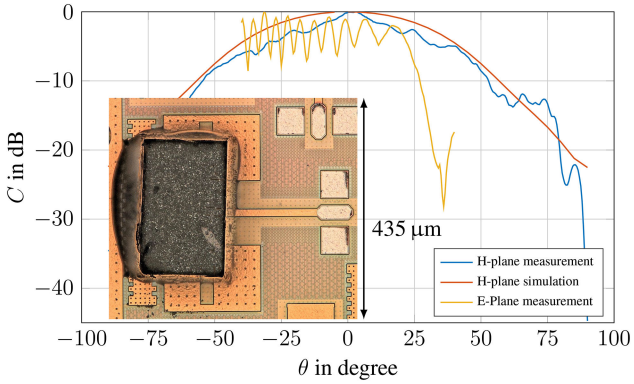

Fig. 7 *Radiation pattern of an integrated antenna at 280 GHz*

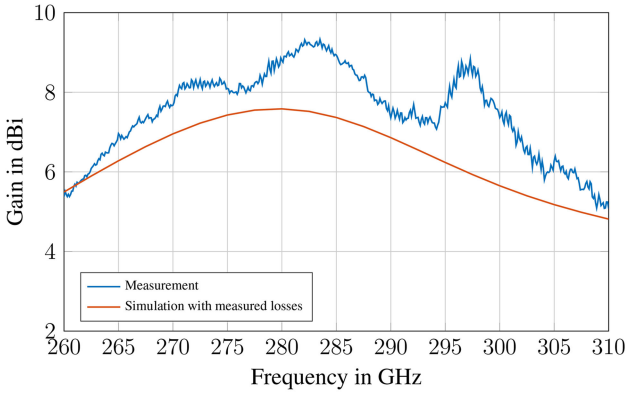

Fig. 8 *Gain of the integrated antenna of Fig. 7*

The body of the wafer probe is mainly made of metal and presents a big reflective surface close to the AUT, causing large ripples in the RP in the *E*-plane as shown in Fig. 7. The amplitude of the ripples causes an uncertainty of u(multiple reflections) = 2.5 dB. Fig. 8 shows the measured and the simulated gain between 260 and 310 GHz. The measured gain at 280 GHz ($G_{\mathrm{AUT}} = 8.7$ dBi) is higher than the simulated gain ($G_{\mathrm{sim}} = 7.6$ dBi), which is due to the maximum in the measured RP (Fig. 7). Another reason could be the narrower main lobe (Fig. 7) compared with the simulation, which also indicates a higher antenna gain.

The expanded uncertainty budget for gain measurements of integrated antenna is 1.7 dB. The phase centre determination did not improve the overall measurement accuracy compared to [10] because the influence of misalignments is comparatively small to the uncertainty caused by probe reflections. One approach to increase the measurement accuracy is to use dedicated probes that are optimised for antenna measurements [20].

6 Conclusion

Phase centre calculations can be used for Rx AUT alignment. With a standard deviation of <50 µm on each axis, this is not only more accurate than measuring with the previously used laser range finder but can also be used for an automatic alignment procedure based on an initial far-field measurement to simplify and quicken the measurement process.

Despite the positional accuracy, the phase centre calculation only had a minor impact on the overall uncertainty budgets, but might have a bigger influence on near field measurements, where the positional accuracy is crucial.

The expanded uncertainty budget was determined forRP, directivity and gain measurements, taking into account mechanical, electrical and post processing errors. Radiation pattern and directivity have an uncertainty budget of 0.2 dB.

With 1.7 dB, gain measurements have the highest uncertainty budget, mainly caused by wafer probe reflections. This can be improved by using wafer probes that are optimised for antenna measurements.

7 Acknowledgment

This work was supported by the German Research Foundation (DFG) under the project number WA 3506/1-1.

8 References

[1] Hitzler, M., Saulig, S., Boehm, L., *et al.*: 'Compact bistatic 160 GHz transceiver MMIC with phase noise optimized synthesizer for FMCW radar'. IEEE Int. Microwave Symp., May 2016

[2] Sarkas, I., Hasch, J., Balteanu, A., *et al.*: 'A fundamental frequency 120-GHz SiGe BiCMOS distance sensor with integrated antenna', *IEEE Trans. Microw. Theory Tech.*, 2012, **60**, pp. 795–812

[3] Novotny, D., Gordon, J., Coder, J., *et al.*: 'Performance evaluation of a robotically controlled millimeter-wave near-field pattern range at the NIST'. 7th European Conf. on Antennas and Propagation (EuCAP), April 2013, pp. 4086–4089

[4] Gulan, H., Beer, S., Diebold, S., *et al.*: 'Probe based antenna measurements up to 325 GHz for upcoming millimeter-wave applications'. Int. Workshop on Antenna Technology (iWAT), March 2013, pp. 228–231

[5] Lee, E.C., Szpindor, E., McKinzie, W.E.III: 'Mitigating effects of interference in on-chip antenna measurements'. AMTA 37th Annual Meeting and Symp., Long Beach, California, USA, October 2015

[6] Gentile, G., Jovanovic, V., Pelk, M., *et al.*: 'Silicon-filled rectangular waveguides and frequency scanning antennas for mm-wave integrated systems', *IEEE Trans. Antennas Propag.*, 2013, **61**, pp. 5893–5901

[7] Tsai, Z.-M., Wu, Y.-C., Chen, S.-Y., *et al.*: 'A V-band on-wafer near-field antenna measurement system using an IC probe station', *IEEE Trans. Antennas Propag.*, 2013, **61**, pp. 2058–2067

[8] Ladds, K.A., Nel, H.P., Stander, T.: 'A novel E-band nearfield scanner for wafer probed on-chip antenna characterisation'. 10th European Conf. on Antennas and Propagation (EuCAP), April 2016, pp. 1–4

[9] Boehm, L., Pledl, S., Boegelsack, F., *et al.*: 'Robotically controlled directivity and gain measurements of integrated antennas at 280 GHz'. European Microwave Conf. (EuMC), Paris, France, September 2015

[10] Boehm, L., Boegelsack, F., Hitzler, M., *et al.*: 'Accuracy evaluation for antenna measurements at mm-wave frequencies'. 10th European Conf. on Antennas and Propagation (EuCAP), April 2016, pp. 1–5

[11] Le Coq, L., Fuchs, B., Kozan, T., *et al.*: 'IETR millimeter-wave compact antenna test range implementation and validation'. 9th European Conf. on Antennas and Propagation (EuCAP), Lisbon, Portugal, April 2015, pp. 1–5

[12] NIST/SEMATECH: 'e-Handbook of Statistical Methods'. http://itl.nist.gov/div898/handbook/mpc/mpc.htm, accessed: 02 October 2015

[13] Beeckman, P.A.: 'Analysis of phase errors in antenna-measurements applications to phase-pattern corrections and phase-centre determination', *IEE Proc. H-Microwaves, Antennas and Propagation*, 1985, **132**, pp. 391–394

[14] Kleine-Ostmann, T., Ulm, D., Schrader, T.: 'Phase center estimation and correction of multi-path effects for the calibration of mm-wave antennas'. 41st Int. Conf. on Infrared, Millimeter, and Terahertz waves (IRMMW-THz), September 2016, pp. 1–2

[15] Newell, A.C., Hindman, G.: 'The alignment of a spherical near-field measurement system using electrical measurements'. IEEE Antennas and Propagation Society Int. Symp. 1998 Digest. Antennas: Gateways to the Global Network. Held in Conjunction with: USNC/URSI National Radio Science Meeting (Cat. No. 98CH36), June 1998, vol. **3**, pp. 1327–1330

[16] Mynster, A.P., Nielsen, J.M., Pivnenko, S.: 'Electrical alignment of antenna coordinate system in a planar near-field setup'. Proc. of the 5th European Conf. on Antennas and Propagation (EUCAP), April 2011, pp. 678–682

[17] Coq, L.L., Lafond, O., Himdi, M.: 'Flip test procedure for positioning system errors and antenna phase centre determinations'. Proc. of the Fourth European Conf. on Antennas and Propagation, April 2010, pp. 1–4

[18] Muehldorf, E.: 'The phase center of horn antennas', *IEEE Trans. Antennas Propag.*, 1970, **18**, pp. 753–760

[19] Hahnel, R., Klein, B., Hammerschmidt, C., *et al.*: 'Distributed on-chip antennas to increase system bandwidth at 180 GHz'. German Microwave Conf. (GeMiC), 2016, pp. 161–164

[20] Boehm, L., Hitzler, M., Roos, F., *et al.*: 'Probe influence on integrated antenna measurements at frequencies above 100 GHz'. European Microwave Conf. (EuMC), London, UK, October 2016